Operational BRDF effects correction for wide-field-of-view optical scanners (BREFCOR)

Schläpfer, Daniel ; Richter, Rudolf ; Feingersh, Tal

Abstract: The radiometric correction of airborne imagery aims at providing unbiased spectral information about the Earth's surface. Correction steps include system calibration, geometric correction, and the compensation for atmospheric effects. Such preprocessed data are affected by the bidirectional reflectance distribution function (BRDF), which requires an additional compensation step. We present a novel method for a surface-coverdependent BRDF effects correction (BREFCOR). It uses a continuous index based on bottom-of-atmosphere reflectances to tune the Ross–Thick Li–Sparse BRDF model. This calibrated model is then used to correct for observation-angle-dependent anisotropy. The method shows its benefits specifically for wide-field-of-view airborne systems where BRDF effects strongly affect image quality. Evaluation results are shown for sample data from a multispectral photogrammetric Leica ADS camera system and for HYSPEX imaging spectroscopy data. The scalability of the procedure for various kinds of sensor configurations allows for its operational use as part of standard processing systems.

DOI: https://doi.org/10.1109/tgrs.2014.2349946

Operational BRDF Effects Correction for Wide-Field-of-View Optical Scanners (BREFCOR)

Daniel Schläpfer, *Member, IEEE*, Rudolf Richter, and Tal Feingersh

***Abstract*—The radiometric correction of airborne imagery aims at providing unbiased spectral information about the Earth's surface. Correction steps include system calibration, geometric correction, and the compensation for atmospheric effects. Such preprocessed data are affected by the bidirectional reflectance distribution function (BRDF), which requires an additional compensation step. We present a novel method for a surface-cover-dependent BRDF effects correction (BREFCOR). It uses a continuous index based on bottom-of-atmosphere reflectances to tune the Ross–Thick Li–Sparse BRDF model. This calibrated model is then used to correct for observation-angle-dependent anisotropy. The method shows its benefits specifically for wide-field-of-view airborne systems where BRDF effects strongly affect image quality. Evaluation results are shown for sample data from a multispectral photogrammetric Leica ADS camera system and for HYSPEX imaging spectroscopy data. The scalability of the procedure for various kinds of sensor configurations allows for its operational use as part of standard processing systems.**

***Index Terms*—Data preprocessing, geophysical image processing, hyperspectral imaging, radiometry, software packages.**

I. Introduction

RECENT airborne optical scanners provide accurate measurements of the at-sensor radiance. The radiometric calibration is feasible to a level of below 3% with respect to absolute standards [1]. However, the analysis of surface characteristics requires an accurate knowledge of its reflectance properties. The calibrated scanner data can be inverted to reflectance quantities using radiative transfer codes such as the moderate resolution atmospheric transmission model MODTRAN-5 [2]. This atmospheric compensation is done in well-established software codes such as ATCOR (atmospheric correction software) [3] or the Fast Line-of-sight Atmospheric Analysis of Spectral Hypercubes [4]. The output of the inversion is a surface reflectance quantity, which is best described as a hemispheric directional reflectance factor (HDRF) [5], [6]. The conical nature of the scanner measurement is neglected due to the very small instantaneous field of view (FOV) of the instrument being close to the infinitesimal theoretical value of directionality of the HDRF. The impact of the variable incidence illumination is accounted for in the topographic correction process using empirical relations combined with calculations of the diffuse and direct irradiance components. Variabilities of the processed imagery due to terrain influences can be thus reduced [7]–[9]. During this process, the hemispherical irradiance field is well approximated by currently available atmospheric compensation methods. The resulting product is close to a true HDRF defined with respect to a fully diffused irradiance field [5]. Influences of the variable irradiance distribution as contained in the "HDRF"-like quantity defined in more recent publications [6] have been mostly removed.

The correction to true HDRF allows for a clear cut between the incidence effects and the observation effects and helps toward a straight forward correction scheme. An alternative to this split approach would be a one-step atmospheric compensation, where bidirectional reflectance distribution function (BRDF) models are coupled directly with the radiative transfer in the atmosphere [10]. In such routines, the number of free variables increases significantly, which has to be paid either by a substantially increased processing time or by introducing fixed parameter assumption for the state of the atmosphere. In this paper, we therefore focus on the sequential approach, where incidence radiance and observation direction are separated on the level of surface HDRF.

The HDRF retrieved after a complete atmospheric compensation is still highly variable due to the influence of the observation angle, i.e., the second direction of the BRDF [5]. The observed directional reflectance value may deviate by up to 50% from the spectral albedo (i.e., from the bihemispherical reflectance (BHR) [5], [6]). The magnitude of this so-called BRDF effect has been confirmed by various measurements, specifically for vegetation and man-made surfaces [11], [12]. Thus, an operational (i.e., automatic, scalable, and readily available) correction method of the HDRF to spectral albedo is of large interest for quantitative remote sensing data analyses.

A number of methods for BRDF correction have been developed in the past: a first group of methods for a flat terrain uses the image statistics in homogeneous terrain. The off-nadir reflectances are normalized by the corresponding scan-angle-dependent brightness values compared with the nadir value [13], [14]. Such algorithms may be also applied to at-sensor radiance data instead of using the bottom-of-atmosphere HDRF. If using the at-sensor radiance, the observation-angle-dependent brightness gradient may be caused by a combination of surface BRDF and "atmospheric BRDF" (i.e., variations due to the asymmetric across-track variability in path radiance). These empirical approaches will correct both effects in one step as long as the image statistics are stable.

Manuscript received January 27, 2014; revised July 3, 2014 and August 5, 2014; accepted August 13, 2014.

D. Schläpfer is with ReSe Applications Schläpfer, 9500 Wil, Switzerland, and also with Kantonsschule, 9500 Wil, Switzerland (e-mail: daniel@rese.ch).

R. Richter is with the German Aerospace Center, 82234 Wessling, Germany.

T. Feingersh is with the MBT Space Division, Israel Aerospace Industries, Yehud 56000, Israel.

Color versions of one or more of the figures in this paper are available online at http://ieeexplore.ieee.org.

Digital Object Identifier 10.1109/TGRS.2014.2349946

Another suite of methods is exclusively dedicated to rugged terrain imagery by topographic correction methods (modified cosine correction, Minnaert correction, enhanced Minnaert approach, statistical–empirical correction) [9], [15]–[17]. These methods correct for BRDF effects due to the variability of the direct and diffuse illumination and the solar incidence angles [8]. The reflectance values of areas with low local solar elevation angles, i.e., large local solar zenith angles, are often overcorrected by the assumption of isotropically reflecting surfaces. The topographic correction methods adjust these values. Specifically, for rugged terrain imagery, it is useful to correct this incidence-angle-dependent BRDF effect, but still, the process should be combined with the correction of the observation-angle-dependent BRDF effect.

The complete BRDF effects can be described by physical or semiempirical models. Such models are employed for the processing of MODIS data [18]–[20], where the BRDF model is fitted to the viewing-angle-dependent image statistics. Similar approaches have been also tested on airborne data by Beisl [21] using a generic model for the whole image. A stratification of the imagery using BRDF classes theoretically improves the accuracy of the BRDF correction. Results of using such models for airborne data have been presented by Weyermann *et al.* [22]. Furthermore, Luo *et al.* [23], [24] and Bréon and Vermote [25] have shown that an aggregation of all pixels from the same land cover type within a small normalized difference vegetation index (NDVI) interval is a valid method to produce the BRDF model parameters for later correction.

The goal of this work is the development and implementation of an operationally usable and generic BRDF correction method. The presented method builds upon the findings in the aforementioned publications. It should be based on a surface cover characterization, which is of continuous nature to avoid classification-related artifacts in the correction. Furthermore, the correction method should rely on one single BRDF model formulation, which can be tuned to the properties of a broad variety of surface cover types. These two preconditions allow calculating a continuous per-pixel anisotropy factor and correcting the HDRF image for the deviations from spectral albedo.

II. BREFCOR Method

A generic routine for the correction of BRDF effects has been implemented, which we name the "BRDF effects correction" method, "BREFCOR" for short. The idea is to apply a scaling of the volume scattering and geometric scattering components within a well-accepted BRDF model. A continuous surface cover index of the complete image is used for this purpose, which covers all surface types from forward scatterers (such as water) to backward scatterers (such as vegetation). The Ross–Thick Li–Sparse (RTLS) reciprocal BRDF model has been selected as basis for the correction of reflectance anisotropy [26]. This model is mainly developed for vegetation, but we use it in a scaled way for all kinds of surfaces. The good performance of this model has been shown for MODIS atmospheric correction by Pokrovsky and Roujean [27], whereas for high-resolution airborne data, no such analysis is known to the authors. For high-spatial-resolution instruments and for specific targets such as water, different models may be applicable as well. However, it was out of the scope of this paper to evaluate the performance of various BRDF models.

A. Selected BRDF Kernels

The BRDF correction scheme is based on the RTLS model, potentially enhanced by the hot spot function as proposed by Maignan *et al.* [28]. For the correction, a formulation of the model for the bidirectional reflectance factor (BRF) is used. The BRF is well suited for correction of the HDRF, as both quantities are defined as 1.0 for a 100% reflecting target at the same observation geometry and as only the second dimension (observation direction) relative variation of the BRF is used for the correction. The generic RTLS equation of the BRF for each pixel and spectral band is given as

$$\rho_{\mathrm{BRF}} = \rho_{\mathrm{iso}} + f_{\mathrm{vol}} K_{\mathrm{vol}} + f_{\mathrm{geo}} K_{\mathrm{geo}} \tag{1}$$

where ρ_{iso} is the isotropic reflectance defined at nadir for both illumination and observation angle. The kernel factors f_{vol} and f_{geo} are weighting coefficients for the respective kernels. They depend on the ground coverage BRDF, whereas the kernels are fixed functions, which define a fully bidirectional reflectance property. The kernels have been selected according to the findings of BRDF literature [18]. For the volume scattering, the Ross–Thick kernel is modified to include the hot spot extension by Maignan, i.e.,

$$K_{\mathrm{vol}} = \frac{4}{3\pi} \frac{1}{\cos\theta_i + \cos\theta_r} \left[\left(\frac{\pi}{2} - \zeta \right) \cos\zeta + \sin\zeta \right] - \frac{1}{3} \tag{2}$$

where $\zeta = \arccos(\cos\theta_i \cos\theta_r + \sin\theta_i \sin\theta_r \cos\phi)$.

The angle θ_i is the incident solar zenith angle, θ_r is the observation zenith angle, and ϕ is the relative azimuth angle $\phi = \phi_i - \phi_r$ (i.e., the difference between incidence and observation azimuth). The extension of this volumetric kernel by Maignan is given as

$$K_{\mathrm{vol}} = \left(K_{\mathrm{vol}} + \frac{1}{3} \right) \left(1 + \frac{1}{1 + \zeta/1.5^\circ} \right). \tag{3}$$

The reciprocal Li–Sparse kernel is used for the geometric part. It is defined as

$$K_{\mathrm{geo}} = \frac{1}{\pi}(t - \sin t \cos t) \left(\frac{1}{\cos\theta_i} + \frac{1}{\cos\theta_r} \right) - \left(\frac{1}{\cos\theta_i} + \frac{1}{\cos\theta_r} \right) + \frac{1 + \cos\zeta}{2\cos\theta_i \cos\theta_r} \tag{4}$$

where t is as defined in the equation shown at the bottom of the page.

$$t = \arccos \left(\frac{\sqrt{\tan^2\theta_i + \tan^2\theta_r - 2\tan\theta_i \tan\theta_r \cos\phi + (\tan\theta_i \tan\theta_r \cos\phi)^2}}{\frac{1}{\cos\theta_i} + \frac{1}{\cos\theta_r}} \right)$$

B. The BRDF Cover Index (BCI)

A continuous BRDF cover index (BCI) function is used for characterization of the surface. It is calculated on the HDRF of four standard bands: blue at 460 nm, green at 550 nm, red at 670 nm, and near infrared at 840 nm. This reduced selection of spectral bands makes the index applicable for most current optical remote sensing systems. The BCI function characterizes the image based on intrinsic BRDF properties from strong forward scatterers (water) to neutral targets (asphalt) to backward scatterers (soils and vegetation types). The index implementation is using the NDVI as a first input for vegetation density quantification due to its known relation to the leaf area index, which has a significant influence on the BRDF [23]. Knowing the limitations of the NDVI for vegetation-type discrimination, we propose an extension of the index to a wider range of surface cover types, i.e., including very dense vegetation and nonvegetated areas in one continuous index. The presented formulation has been found empirically.

The NDVI is increased in (5) by a value of up to 0.5 using the fact that dense agricultural vegetation shows higher green reflectance than dense forests; i.e., the NDVI is increased by C_{forest} for dense forests having green reflectance in a range below 7%. In a further step, the BCI is decreased for soils by C_{soils} using the effect that soils show relatively low blue at-sensor radiance. A last adaption C_{water} is made for water such that clear water areas are always set to a minimum value, i.e.,

$$\mathrm{BCI} = (\mathrm{NDVI} + C_{\mathrm{forest}} - C_{\mathrm{soils}} - C_{\mathrm{water}}) > -1.2. \quad (5)$$

Note that the ">" sign denotes a maximum operator between the left and right sides of the term.

The three correction functions in (5) are given in the following; first, for forests using the absolute HDRF value in the green ρ_{green}

$$C_{\mathrm{forest}} = \frac{0.5}{0.04 \cdot 0.2} \cdot \left([0.07 - \rho_{\mathrm{green}}]_{0.00}^{0.04} \right) \cdot \left([\mathrm{NDVI} - 0.55]_{0.00}^{0.20} \right). \quad (6)$$

The upper and lower values at the square brackets indicate a truncation at these values. The upper values could be adapted for better representation of biome types. For surface covers having a BCI below 0.1 (i.e., mostly soils), a reduction factor is found from the relation between blue and red HDRFs as

$$C_{\mathrm{soils}} = \frac{\rho_{\mathrm{blue}}}{\rho_{\mathrm{red}}} \left([1 - 10 \cdot (\mathrm{NDVI} + C_{\mathrm{forest}})]_{0.00}^{1.00} \right). \quad (7)$$

This factor accounts for the variability of nonvegetated areas in the visible. Finally, a summand to account for water is added, starting with $\mathrm{BCI}_{\mathrm{soil}} = \mathrm{NDVI} + C_{\mathrm{forest}} - C_{\mathrm{soils}}$. It takes into account the relatively higher reflectance of water in the green spectral band in relation to the blue band for discrimination to other surface targets such as shadows and dark asphalt, i.e.,

$$C_{\mathrm{water}} = \left(\left(\frac{\rho_{\mathrm{green}}}{2\rho_{\mathrm{blue}}} - 0.8 \right) > 0 \right) \cdot \left(-3 \left((\mathrm{BCI}_{\mathrm{soil}} + 0.5) > 0 \right) \right). \quad (8)$$

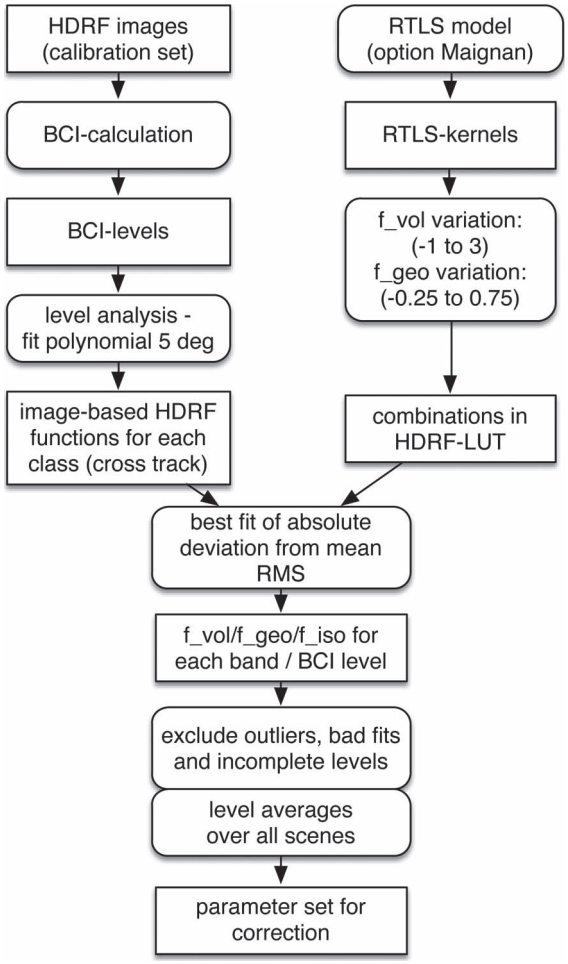

Fig. 1. BRDF model calibration scheme using BCI-based image stratification and the RTLS model.

The range of the final BCI function is defined between values of -1.20 and 1.50. The BCI calculated in each image pixel can be then used for BRDF model calibration and, subsequently, for image correction.

C. Model Calibration

The BRDF model requires kernel weighting factors for both the geometric and volumetric kernels of the RTLS model. These factors vary depending on surface cover types and phaenological state. Finding the correct kernel weighting factors for a data set acquired under the same conditions and in the same geographical region is what we call the BRDF model calibration. Using the overlap between two images would potentially lead to a valid model calibration [29]. However, the BREFCOR method does not make use of this option due to limitations of such an approach in operational use over heterogeneous landscapes. Rather, it calculates the kernel weightings at first for each scene independently.

For the calibration of the model, a number of suited calibration scenes is first selected, as one single scene usually does not cover all relevant surface cover types across the full across-track direction (compare Fig. 1). For the single-scene calibration, the kernels are reduced to two dimensions by selecting the values for the given solar zenith and azimuth

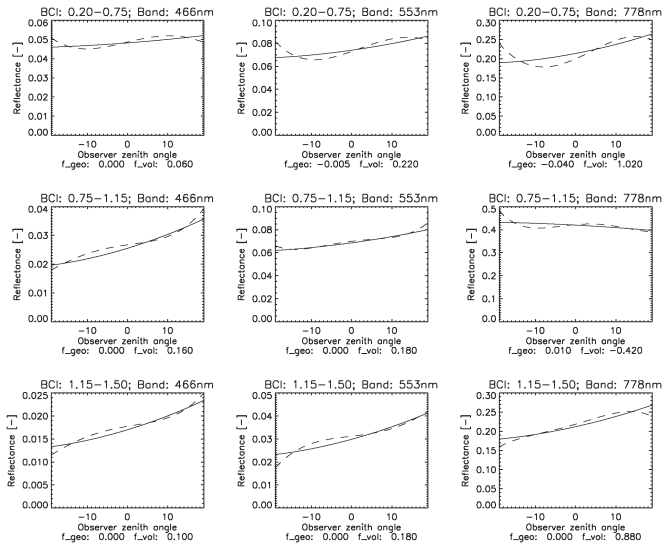

Fig. 2. Model calibration example for three levels of BCI and three selected spectral bands (based on HYSPEX data); the dashed line is the polynomial across-track HDRF variation, and the solid line is the respective model fit.

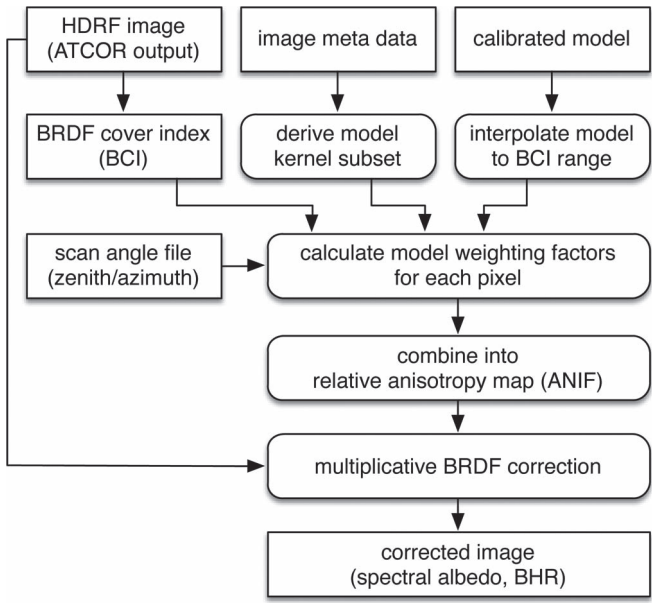

Fig. 3. Image BRDF anisotropy correction scheme based on the calibrated BRDF model.

only. A 1-D kernel function depending on the occurring off-nadir sensor zenith angle range is then found using the flight heading parameter. The absolute azimuth angle, averaged for each off-nadir column, is included in the analysis to correct for the sensor along-track tilt. The BCI of the scene is then stratified into a number of four to seven levels (compare Section V-A). The across-track variation of the HDRF for each BCI level is first fitted to a polynomial of the fifth degree. This function is then compared with the systematically varied observation BRF model by systematic variations of the weighting factors in the RTLS model. The best fit between the observed function and the RTLS model is found by RMS calculation. Such found optimum kernel weights are stored for each scene and each BCI level of the calibration data set. A combined BRDF model is then created by averaging all weights from the various scenes on the same BCI level. Bad-fitting levels (with relative RMS errors greater than 12% in reflectance) and outliers, which are more than 100% off the mean, are excluded from averaging. The BRDF correction parameters are set to "isotropic" for BCI levels without any fitting parameters. Such averaged model is finally stored for later application to the imagery. Note that cloud pixels are excluded for the calibration process using a preclassification map of haze, cloud, and water as created during the atmospheric compensation.

The critical parameter in this calibration process is the selection of appropriate BCI levels for the calibration. Our evaluation on many scenes has shown that increasing the number of calibration levels often leads to worse fitting results and less stable BRDF correction, whereas keeping the number of levels small is more stable. A second outcome was that it is hardly feasible to define generic calibration limits for all kinds of data acquisition and sensors. Thus, the calibration level limits should be adjustable in a flexible way.

An example of this fitting procedure results is given in Fig. 2 for three BCI levels using a moderate FOV instrument (compare Section V-B). The across-track variation on each of the levels is interpolated by a polynomial fifth degree, and the fitting is done to this function. Using a function for the fit instead of single points helps, on one hand, to avoid potential asymmetric weighting of the function in across-track direction and, second, to minimize the influence of outliers.

D. Image Correction

Finally, the derived BRDF model calibration data are applied to the image data. For application on the imagery, the BCI has to be calculated from each image to get a continuous correction factor.

The image processing procedure is following these steps (compare Fig. 3).

- Calculate the BCI from image.
- Calculate the scene-specific angular kernels subsets.
- Interpolate the calibration data from BCI levels to a continuous BRDF model.
- Calculate an anisotropy map by scaling the kernels using the BCI, the scan angles (observation zenith and azimuth angle), and the interpolated BRDF model.
- Apply the anisotropy map on a per-pixel basis.

The anisotropy factor is derived as the relation of the directional model for each pixel to the same model averaged over all angles (i.e., to a good approximation of the spectral albedo BHR), i.e.,

$$\mathrm{ANIF} = \frac{\rho_{\mathrm{iso}} + f_{\mathrm{geo}} K_{\mathrm{geo},\theta_i,\theta_r,\phi} + f_{\mathrm{vol}} K_{\mathrm{vol},\theta_i,\theta_r,\phi}}{\rho_{\mathrm{iso}} + f_{\mathrm{geo}} \overline{K_{\mathrm{geo}}} + f_{\mathrm{vol}} \overline{K_{\mathrm{vol}}}} \approx \frac{\rho_{\mathrm{BRF}}}{\rho_{\mathrm{BHR}}}. \tag{9}$$

The BHR is described by the two hemispherical averages $\overline{K_{\mathrm{geo}}}$ and $\overline{K_{\mathrm{vol}}}$ weighted by the respective factors and added to the constant isotropic reflectance ρ_{iso}. Alternatively, the anisotropy with respect to nadir BRF would be an option as done in earlier BRDF research [30]. This option is currently not supported in BREFCOR, as the BHR is the more generic spectral albedo definition for surface object characterization.

The corrected BHR is finally calculated as $\rho_{\mathrm{BHR}} = \rho_{\mathrm{HDRF}}/\mathrm{ANIF}$, where ρ_{HDRF} is the bottom-of-atmosphere (directional) reflectance after standard ATCOR-4 atmospheric compensation, as described above.

III. Implementation

The method has been implemented in the interactive data language (IDL) [31] and is embedded in the ATCOR atmospheric compensation software. It makes use of the predefined layers available from the atmospheric compensation process, such as observation scan angles, the cloud mask, and the atmospheric and geometric meta data as stored in the ATCOR process. The incidence BRDF correction is done by the semiempirical approach during the atmospheric compensation process, as mentioned in the introduction of this paper. The BREFCOR process is a straightforward implementation starting sequentially after full atmospheric correction to HDRF. The calibration of the BRDF model can be done on four to seven BCI levels, using defaults or self-defined index limits for stratification. As the selected levels are cover types specific, the calibration limits can be tested on a three-band image subset until an optimum is found for a region or campaign. This model parameters can be then stored and applied to large-scale image data.

The total processing time on a 2.2-GHz Intel quad core i7 processing system is approximately 50 min for a set of three imaging spectroscopy scenes (dimensions approximately 1500×6000 pixels each, 199 spectral bands; a total of 9.5 GB of data). The model calibration takes 21 min in this case for seven calibration levels and all spectral bands, whereas the image processing is between 8 and 10 min per scene for this example. Thus, the data throughput is 5–6 min per gigabyte of data. This is comparable with the processing time required for the atmospheric compensation step (including topography), i.e., the processing time for the radiometric compensation is doubled if a BRDF correction is executed.

The implementation has been optimized for large-volume processing for the ADS-80 system operated by the Swiss Federal Institute of Topography (swisstopo) in conjunction with an implementation of the ATCOR-4-based workflow. Interfaces have been created for both experimental data analysis through an IDL-based graphical user interface and for text-file-based batch processing. The implemented operational preprocessing system includes the ATCOR-4 based atmospheric compensation process to HDRF and the BREFCOR BRDF correction process. It fulfills the following requirements: 1) full support for automatic batch mode operation; 2) batch call for a series of images in the same area; 3) automatic meta data handling; 4) detailed process logging; 5) consistent error handling; and 6) layout for parallel processing of various series. Operational use of this ATCOR-4 processing system has started in May 2014.

IV. Test Data

The BREFCOR method has been tested successfully on a variety of airborne imaging spectroscopy data. I could be shown that the method works for vegetated and nonvegetated areas alike, reducing the relative difference for various observation angles by a factor of 2 [32]. The applicability has been also shown on multispectral small FOV satellite data [33], where nine image scenes of different observation angles could be corrected by the model. In this paper, we focus on the evaluation of an airborne photogrammetric camera system (Leica ADS-80 [34]) and an imaging spectroscopy system (HYSPEX [35]). Both systems are providing calibrated at-sensor radiance values, which can be processed by radiative transfer model inversion in an operational fully automatic process. The FOVs of these sensors differ significantly, but both instruments use a total FOV larger than 20°, which is well suited to fit a BRDF model. As of our experience, the BRDF variations in smaller FOVs tend to be hardly discernible from natural systematic variations, and image noise and results become less stable.

A. ADS Data

The Leica ADS-80 camera (airborne digital camera system) scans the Earth in nadir view using four spectral bands (477, 558, 634, and 867 nm). The total FOV angle of the system is 46° and is covered by 12 000 across-track pixels [34]. With flight altitudes between 1000 and 3000 m above ground, this results in a standard resolution of 0.25 m after standard geometric processing using the Leica GPro software. For remote sensing applications, the data set is reprocessed on a resolution of 2 m. Two such systems are operated by the swisstopo for regular data acquisition and mapping applications. The cameras are validated on a yearly basis such that the absolute radiometric calibration is well controlled. Standard data acquisition is done in east-west direction, mainly due to topographical reasons. The wide FOV and the chosen flight directions result in strong BRDF effects. For the development of the BREFCOR method, a total of five data sets has been investigated from both spring time and midsummer vegetation state and from agricultural, mountainous, and mostly forested areas. Hereafter, results are shown from a 0.25-m resolution data set, which showed the strongest BRDF effects of the data sets investigated. The data were acquired in March 2012 at the Swiss/German border (Dogern) at a solar zenith angle of 49.7° and an azimuth angle of 205.1°, respectively (compare Fig. 4). It has been atmospherically corrected by the ATCOR-4 model using a standard 25-m-resolution digital terrain model.

B. HYSPEX Data

The second validation data set is based on HYSPEX imagery [35]. The system is operated by the German Aerospace Center (DLR). The HYSPEX VNIR-1024 imaging spectroscopy system scans the surface with a total FOV of 34° in 160 contiguous bands for the visible and near-infrared spectral range from 410 to 990 nm. The spatial resolution of the georectified product was at 0.6 m at a flight altitude of approximately 1000 m above ground. The sample data consist of a total of five data strips, which were acquired over the Kaufbeuren test site in Southern Germany on July 8, 2013; the sun was at 41° zenith angle and 113° azimuth angle. Some clouds were present in the data, which inhibited the use of all data strips for our test. The data were georectified using DLR's orthorectification software

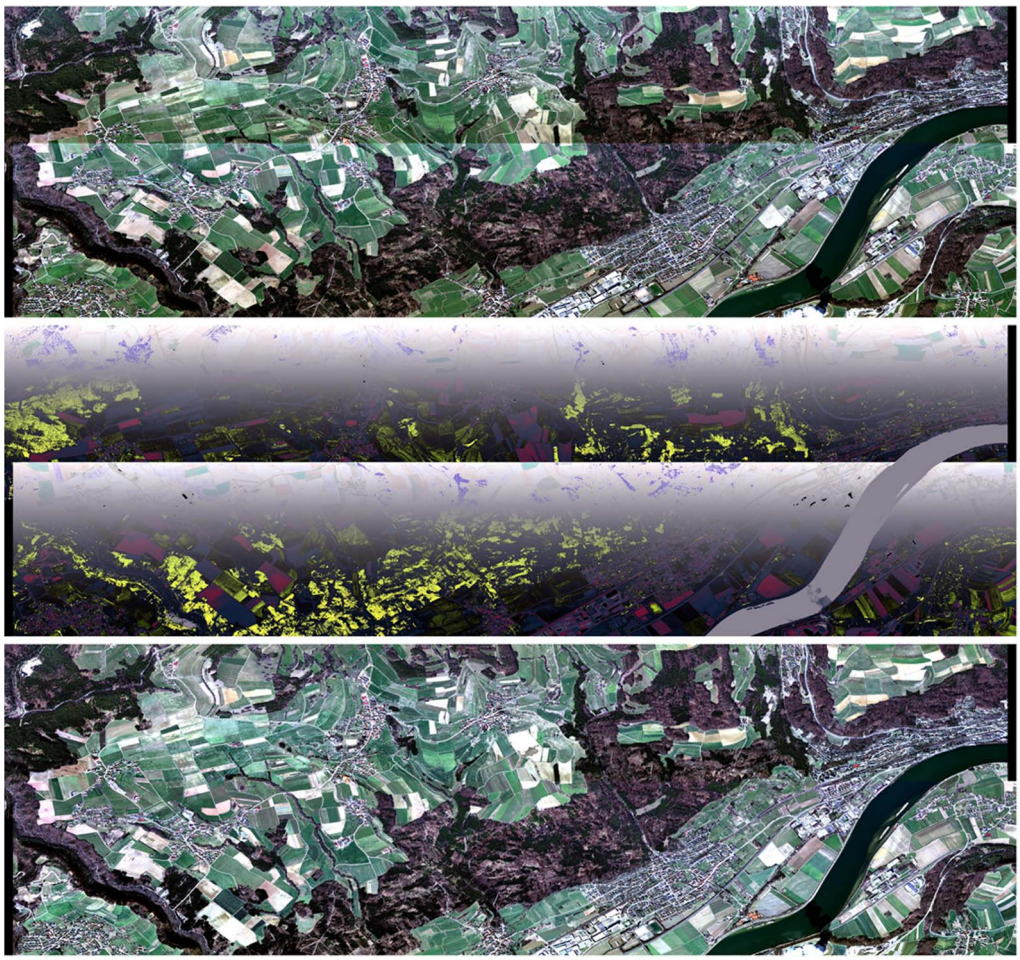

Fig. 4. BREFCOR correction. (Top) Uncorrected HDRF (RGB display). (Middle) Anisotropy factor as three-band RGB in a range of ∼0.8 (black) to ∼1.2 (white). (Bottom) Corrected BHR. ADS-80 image mosaic, reproduced by permission of swisstopo [BA13124].

[36], and atmospheric compensation to bottom-of-atmosphere HDRF was performed by ATCOR-4.

V. Results of Validation

The results of the two aforementioned representative samples are shown and validated here.

A. Airborne Digital Photogrammetry Data (ADS-80)

The mosaic of the two east-west flown flights of Leica ADS data is depicted in Fig. 4. The data are affected by strong across-track gradients after atmospheric compensation (top image). The middle image is the continuous surface-cover-dependent anisotropy factor used for the correction. The range of calculated ANIF values is between 0.8 and 1.2 for red, green, and near infrared; whereas for the blue band, a higher variation of 0.7 to 1.25 has been observed. For water surfaces (BCI < -1.2), the anisotropy was forced to 1, i.e., no correction is done over water as the model calibration is unstable for this BCI level based on these two scenes. The tests on these very high resolution ADS-80 data have shown that the higher spatial resolution (i.e., 0.25 m) combined with the large FOV (across-track FOV) of this system allows for a more accurate calibration of the model using six levels, whereas for the reduced spatial resolution (i.e., 2 m) five levels proved to lead to better calibration results. The better resolution reduces the averaging effect of spectra, and thus, the surfaces cover types can be better discriminated for calibration.

The lower image is the correction result based on the calibrated RLTS BRDF model. Most BRDF effects can be removed by this method as long as the image statistics allow for a good model calibration. However, shaded areas in forests are still affected by visible differences due to the variable spatial shadow structure if seen from varying angles. The number of full cast shadow pixels varies significantly between the observation angles at high resolutions—something that cannot be corrected by a pixel-based BRDF correction.

The radiometric changes in the process are depicted in Fig. 5. The spectra of two overlapping samples in the image are shown before and after radiometric correction. The atmospheric correction changes the shape of the spectra from at-sensor radiance to bottom-of-atmosphere reflectance. However, the BRDF-related offset remains. This variability is then removed by the BREFCOR correction step. The impact of the BRDF correction is analyzed in more detail using an overlap of two scenes (compare Fig. 6 for a chessboard overlay of the two images). A linear fit is done between all overlapping pixels, such that the linearity, as shown in Table I, would ideally be at 1. The

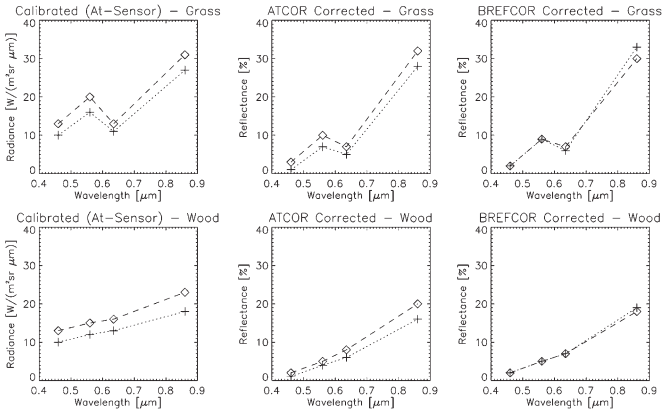

Fig. 5. Sample results for two selected targets of ADS four-band imagery in the overlapping range of two adjacent images, seen from two angles. (Left) Calibrated at-sensor radiance. (Middle) ATCOR atmospheric compensation (HDRF). (Right) BREFCOR corrected BHR.

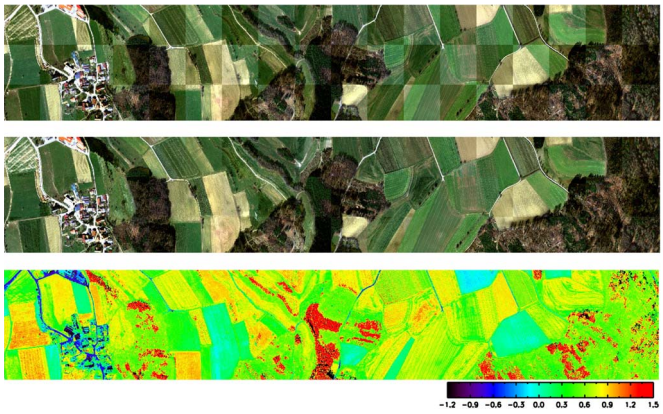

Fig. 6. (Top) Uncorrected chessboard in overlay region (RGB). (Middle) BREFCOR corrected. (Bottom) BCI. ADS image subset reproduced by permission of swisstopo [BA13124].

TABLE I
IMPACT OF BREFCOR CORRECTION ON THE RELATION BETWEEN IMAGERY IN THE OVERLAP REGION FOR THE ADS-80 SAMPLE IMAGE

Band	ATCOR (HDRF)		BREFCOR (BHR)	
	Offset [%]	Linearity	Offset [%]	Linearity
Blue	0.1	0.71	1.5	1.04
Green	2.0	0.74	1.9	1.00
Red	1.5	0.83	1.4	1.06
NIR	3.3	0.81	4.3	1.00

numbers show the quantitative impact of the BRDF correction on the linear relation between the same pixels acquired from two different observation angles. A difference of almost 30% in linearity is apparent in the uncorrected case, which is reduced to about 6% after BREFCOR correction, whereas the offsets remain more or less unchanged.

B. Imaging Spectroscopy Data (HYSPEX)

For the HYSPEX data, each of the 160 spectral bands is individually calibrated using six levels with calibration limits for dense summer vegetation. The calibration limits have to be defined differently compared with the ADS data, since the vegetation status is differing significantly for the summer acquisition time: more levels for dense vegetation had to be

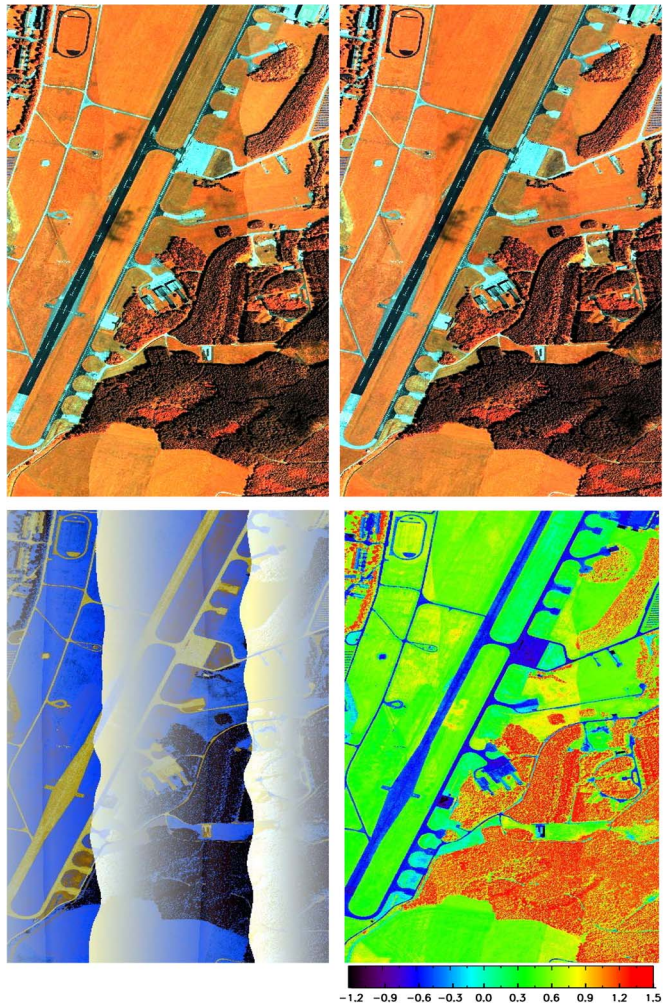

Fig. 7. BREFCOR correction mosaic of three HYSPEX image lines in bands NIR (807 nm), green (550 nm), and blue (459 nm). (Top left) Uncorrected HDRF. (Top right) Corrected BHR. (Bottom left) Anisotropy factor (blue–green–NIR display, variation from dark at ∼0.9 to bright at ∼1.05). (Bottom right) BCI. (HYSPEX images, (c) DLR).

defined for the calibration of the model. In addition, the BRDF model calibration did not work satisfyingly on all three strips as thin clouds had been present in one of the strips; this scene therefore had to be excluded from the model calibration step for better results. A sample result of this correction is shown in Fig. 7. The calculated anisotropy was between 0.9 and 1.05 for most of the bands. The variation was slightly higher for the near-infrared bands and in the blue band. BRDF effects are well removed for the vegetation areas, whereas the concrete runways remain mostly untouched.

A more detailed analysis is made in the overlap region of the two images. This validation is done on selected spectra and in a statistical way. The comparison of two selected samples of grass and forest is shown in Fig. 8. Spectra are clearly closer to each other after correction, whereas the differences are significantly reduced. A statistical evaluation is done based on the full overlap area by a pixel-by-pixel comparison. A low-pass filter of five pixels is applied before the analysis to avoid coregistration-related noise in the calculated differences. Furthermore, the influence of the systematic geometric coregistration error has been included in the analysis with RMS

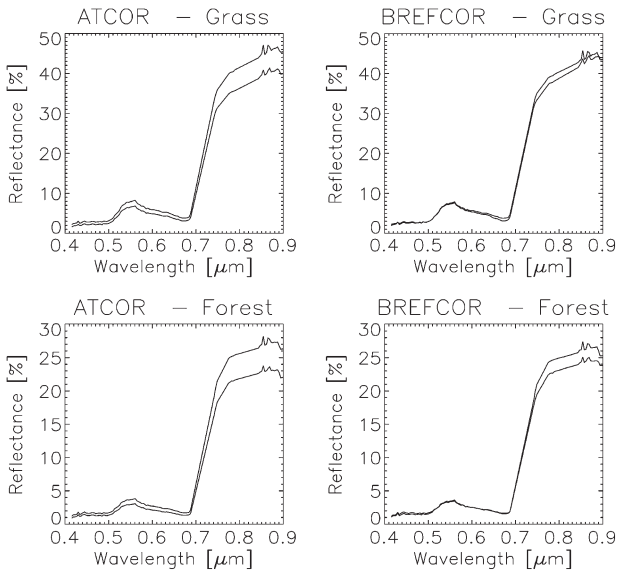

Fig. 8. Samples of spectra of the same grass and forest region of interest from two overlapping HYSPEX images before and after BREFCOR correction. (Left) HDRF values. (Right) BHR values.

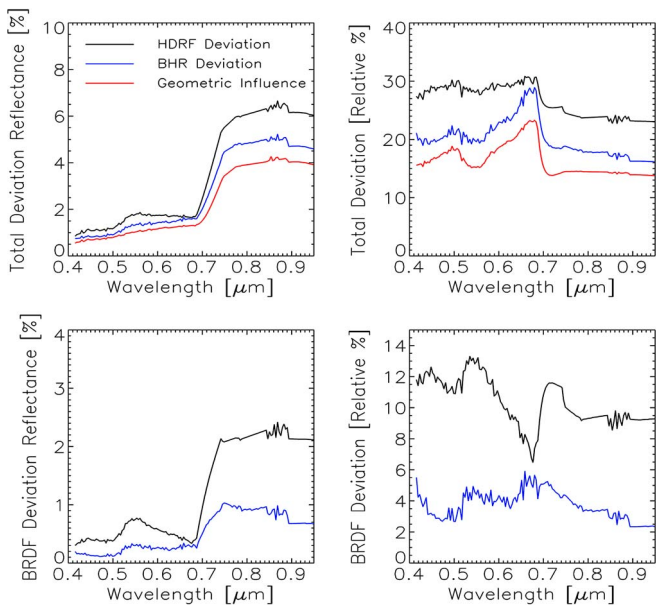

Fig. 9. Statistical evaluation of the overlap area of two HYSPEX images, band averages of complete overlapping area. (Top left) Total deviation in reflectance units. (Top right) Relative deviation from band mean reflectance. (Bottom images) Same deviations after correction for the impact of geometric coregistration influence.

accuracy of the relative coregistration at 2.4 pixels (known from cross-correlation analysis). The impact of this geometric offset was simulated by taking the average difference when shifting the filtered image by two pixels. This simulated error was then subtracted from the total deviations, which results in a good estimate of the deviation, which can be mainly attributed to BRDF influences. The results (see Fig. 9) show the improvements due to the correction. The absolute error in reflectance could be reduced by a factor of 2 and more, whereas the relative error improved from about 10% to 4% for most of the spectral range. It is interesting to note that the correction did not significantly change the spectrum at the maximum chlorophyll absorption around 680 nm. A larger variability and an increased cross sensitivity are immanent at this wavelength due to the low absolute signal. Thus, the automatic calibration routine could not find well-fitting BRDF model parameters, which resulted in a reduced correction.

A last check is done for the grass signature by comparing the image-based model results with laboratory goniometer measurements [12]. The anisotropy factor is plotted for both the model results from image and the laboratory BRDF in Fig. 10. The figure is arranged such that the solar principle plane is in the vertical direction. The displayed anisotropy has been calculated in relation to the hemispherical integral of the BRFs. The image-based model calibration is limited to the maximum off-nadir observation zenith angle of $\pm 17°$; i.e., all modeled values beyond these limits are derived by extrapolation using the model. The plot proves the stability of the model as no extrapolation artifacts are occurring. The real-world measurements show more significant anisotropy than the model. Hot spot characteristics and punctual shadowing artifacts cannot be reconstructed by the model. Nevertheless, the data range and the generic distribution are well comparable between model and laboratory measurements. The figure corroborates that the found model is of conservative nature as the anisotropy used for image correction is lower than the real-world BRFs.

VI. Conclusion

A novel BRDF correction framework has been implemented as an additional processing step after standard atmospheric compensation. The presented BREFCOR model allows correcting optical remote sensing data having at least four spectral bands in the visible and near infrared for the major influences of BRDF effects and brings the processed data closer to the spectral albedo representation. The first version of the method is implemented and available for use within the ATCOR preprocessing software. Tests have been performed on both multispectral and hyperspectral airborne remote sensing data from both vegetated areas and nonvegetated surfaces. In most cases tested so far, the method leads to improved stability of surface reflectance data with respect to the observation angle. Reduced accuracies of the resulting images have been only found if calibration of the BRDF models was performed on inappropriate reference imagery or if the solar zenith angle was very large (i.e., above 60°). The method has clear limitations on water, snow surfaces, and in urban environments—further research would be required to investigate possible solutions for these targets.

Based on the presented method, a fully automatic (i.e., operational) system has been implemented as part of the ADS-80 processing chain at the swisstopo. It is used for automatic processing of remote sensing products from airborne digital photogrammetric data. The BREFCOR method could be implemented together with the ATCOR-4 process for large-scale data processing. The first results have shown a high degree of scalability in this operational environment, whereas more experience for this large-scale situation is still to be gained.

An extension of the method would be to correct the BRDF effect in a two-step iterative method as proposed in [37];

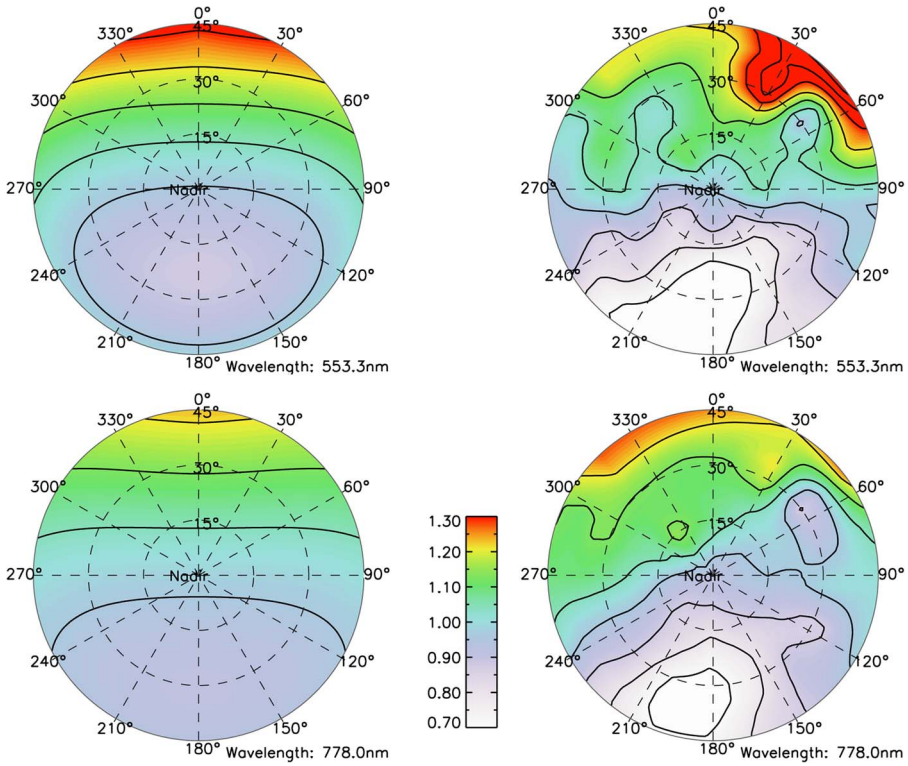

Fig. 10. Anisotropy factor at an incidence zenith angle of 41° in the HYSPEX situation. (Left) Simulation using calibration from three HYSPEX scenes for the grass-like spectra. (Right) Laboratory measurements of a grass sample [12].

specifically, the calculation of the BCI could benefit from such an iteration as it relies on absolute reflectance values. This option has not yet been followed due to the currently encountered limitations in terms of processing time: an iteration would potentially double the time demand for the given method.

Another potential improvement to be envisaged is the inclusion of the digital elevation model slope and aspect information. Depending on surface type, the observation angles would need to be adapted by the local surface tilt in order to get the correction factors in rugged terrain. Furthermore, the use of spectral autocorrelation rules would help to improve BRDF correction in strong absorption features such as in the chlorophyll absorption band. The reliability of the correction is reduced in these bands due to the lower signal and higher cross sensitivity, and thus, BRDF information from neighbor spectral positions could be propagated to fill these gaps.

The method as described in here can be also applied to multiangle satellite imagery, given that a series of images is acquired during a similar time of the year in a way, as shown by Lyapustin *et al.* [38]. A respective adaptation of the BREFCOR method has been included in the satellite version of ATCOR, and first tests on multiangle satellite data show promising results. Further validation of this second type of BRDF correction is still ongoing. Nevertheless, the BREFCOR correction framework is implemented now and is available to end users for their own testing. Further experience will be gained, and improvements as outlined in the conclusions will now be gradually added in order to further advance BREFCOR for both scientific and operational use.

Acknowledgment

The authors would like to thank swisstopo for the support on this project. They would also like to thank J. Weyermann from RSL Zürich for the valuable inputs, E. Ben-Dor from Tel Aviv University for the goniometry data, and the German Aerospace Center (DLR) for providing the HYSPEX data.

References

[1] P. Gege *et al.*, "Calibration facility for airborne imaging spectrometers," *ISPRS J. Photogramm. Remote Sens.*, vol. 64, no. 4, pp. 387–397, Jun. 2009.

[2] A. Berk *et al.*, "MODTRAN5: A reformulated atmospheric band model with auxiliary species and practical multiple scattering options," in *Proc. SPIE*, S. S. Shen and P. E. Lewis, Eds., 2004, pp. 341–347.

[3] R. Richter and D. Schläpfer, "Geo-atmospheric processing of airborne imaging spectrometry data. Part 2: Atmospheric/topographic correction," *Int. J. Remote Sens.*, vol. 23, no. 13, pp. 2631–2649, Jan. 2002.

[4] T. Perkins *et al.*, "Speed and accuracy improvements in FLAASH atmospheric correction of hyperspectral imagery," *Opt. Eng.*, vol. 51, no. 11, pp. 111 707-1–111 707-7, Jun. 2012.

[5] F. E. Nicodemus, J. C. Richmond, J. J. Hsia, I. W. Ginsberg, and T. Limperis, *Geometrical Considerations and Nomenclature for Reflectance*. Washington, DC, USA: U.S. Department Of Commerce, National Bureau Of Standards, 1977.

[6] G. Schaepman-Strub, M. Schaepman, T. Painter, S. Dangel, and J. Martonchik, "Reflectance quantities in optical remote sensing—Definitions and case studies," *Remote Sens. Environ.*, vol. 103, no. 1, pp. 27–42, Jul. 2006.

[7] R. Richter, "Correction of satellite imagery over mountainous terrain," *Appl. Opt.*, vol. 37, no. 18, pp. 4004–4015, Jun. 1998.

[8] R. Richter, T. Kellenberger, and H. Kaufmann, "Comparison of topographic correction methods," *Remote Sens.*, vol. 1, no. 3, pp. 184–196, Jul. 2009.

[9] I. Sola, M. Gonzalez-Audicana, J. Alvarez-Mozos, and J. L. Torres, "Synthetic images for evaluating topographic correction algorithms," *IEEE Trans. Geosci. Remote Sens.*, vol. 52, no. 3, pp. 1799–1810, Mar. 2014.

[10] V. C. E. Laurent, W. Verhoef, J. G. P. W. Clevers, and M. E. Schaepman, "Inversion of a coupled canopy–atmosphere model using multi-angular top-of-atmosphere radiance data: A forest case study," *Remote Sens. Environ.*, vol. 115, no. 10, pp. 2603–2612, Oct. 2011.
[11] S. R. Sandmeier, "Acquisition of bidirectional reflectance factor data with field goniometers," *Remote Sens. Environ.*, vol. 73, no. 3, pp. 257–269, Sep. 2000.
[12] T. Feingersh, "Aspects of reflectance anisotropy and its propagated influence on analysis of urban dynamics," Ph.D. dissertation, Tel-Aviv University, Tel Aviv, Israel, 2007.
[13] R. E. Kennedy, W. B. Cohen, and G. Takao, "Empirical methods to compensate for a view-angle-dependent brightness gradient in AVIRIS imagery," *Remote Sens. Environ.*, vol. 62, no. 3, pp. 277–291, Dec. 1997.
[14] U. Beisl and N. Woodhouse, "Correction of atmospheric and bidirectional effects in multispectral ADS40 images for mapping purposes," in *Proc. ISPRS IAPRS*, O. Altan, Ed., 2004, vol. XXXV, pp. 1–5, Comission VII, WG VII. Istanbul: ISPRS.
[15] P. M. Teillet, B. Guindon, and D. G. Goodenough, "On the slope-aspect correction of multispectral scanner data," *Can. J. Remote Sens.*, vol. 8, no. 2, pp. 84–106, Dec. 1982.
[16] D. Riano, E. Chuvieco, J. Salas, and I. Aguado, "Assessment of different topographic corrections in Landsat-TM data for mapping vegetation types," *IEEE Trans. Geosci. Remote Sens.*, vol. 41, no. 5, pp. 1056–1061, May 2003.
[17] S. A. Soenen, D. R. Peddle, and C. A. Coburn, " SCS+C: A modified sun-canopy-sensor topographic correction in forested terrain," *IEEE Trans. Geosci. Remote Sens.*, vol. 43, no. 9, pp. 2148–2159, Sep. 2005.
[18] W. Wanner *et al.*, "Global retrieval of bidirectional reflectance and albedo over land from EOS MODIS and MISR data: Theory and algorithm," *J. Geophys. Res.*, vol. 102, no. D14, pp. 17 143–17 161, Jul. 1997.
[19] B. Hu, W. Lucht, and A. H. Strahler, "The interrelationship of atmospheric correction of reflectances and surface BRDF retrieval: A sensitivity study," *IEEE Trans. Geosci. Remote Sens.*, vol. 37, no. 2, pp. 724–738, Mar. 1999.
[20] W. Lucht, C. B. Schaaf, and A. H. Strahler, "An algorithm for the retrieval of albedo from space using semiempirical BRDF models," *IEEE Trans. Geosci. Remote Sens.*, vol. 38, no. 2, pp. 977–998, Mar. 2000.
[21] U. Beisl, "Simultaneous correction of bidirectional effects in line scanner images of rural areas," in *Remote Sensing for Environmental Monitoring, GIS Applications, Geology II*, vol. 4886, *International Society for Optics and Photonics*, M. Ehlers, Ed. Bellingham, WA, USA: SPIE, 2003, pp. 551–560.
[22] J. Weyermann, A. Damm, M. Kneubühler, and M. Schaepman, "Correction of reflectance anisotropy effects of vegetation on airborne spectroscopy data and derived products," *IEEE Trans. Geosci. Remote Sens.*, vol. 52, no. 1, pp. 616–627, Jan. 2013.
[23] Y. Luo, A. P. Trishchenko, R. Latifovic, and Z. Li, "Surface bidirectional reflectance and albedo properties derived using a land cover-based approach with moderate resolution imaging spectroradiometer observations," *J. Geophys. Res., Atmos.*, vol. 110, no. D1, pp. 2156–2202, Jan. 2005.
[24] Y. Luo, A. P. Trishchenko, and K. V. Khlopenkov, "Developing clear-sky, cloud and cloud shadow mask for producing clear-sky composites at 250-meter spatial resolution for the seven MODIS land bands over Canada and North America," *Remote Sens. Environ.*, vol. 112, no. 12, pp. 4167–4185, Dec. 2008.
[25] F.-M. Bréon and E. Vermote, "Correction of MODIS surface reflectance time series for BRDF effects," *Remote Sens. Environ.*, vol. 125, pp. 1–9, Oct. 2012.
[26] B. Hu, W. Lucht, X. Li, and A. H Strahler, "Validation of kernel-driven semiempirical models for the surface bidirectional reflectance distribution function of land surfaces," *Remote Sens. Environ.*, vol. 62, no. 3, pp. 201–214, Dec. 1997.
[27] O. Pokrovsky and J.-L. Roujean, "Land surface albedo retrieval via kernel-based BRDF modeling: I. Statistical inversion method and model comparison," *Remote Sens. Environ.*, vol. 84, no. 1, pp. 100–119, Jan. 2003.
[28] F. Maignan, F. M. Bréon, and R. Lacaze, "Bidirectional reflectance of Earth targets: Evaluation of analytical models using a large set of spaceborne measurements with emphasis on the hot spot," *Remote Sens. Environ.*, vol. 90, no. 2, pp. 210–220, Mar. 2004.
[29] S. Collings, P. Caccetta, N. Campbell, and X. Wu, "Techniques for BRDF correction of hyperspectral mosaics," *IEEE Trans. Geosci. Remote Sens.*, vol. 48, no. 10, pp. 3733–3746, Oct. 2010.
[30] S. T. Sandmeier and D. W. Deering, "Structure analysis and classification of boreal forests using airborne hyperspectral BRDF data from ASAS," *Remote Sens. Environ.*, vol. 69, no. 3, pp. 281–295, Sep. 1999.
[31] Exelis Visual Information Solutions. IDL Software-Interactive Data Language, Boulder, CO, USA 2012. [Online]. Available: http://www.exelisvis.com/ProductsServices/IDL.aspx
[32] D. Schläpfer and R. Richter, "Evaluation of BRECOR BRDF effects correction for Hyspex, CASI, APEX imaging spectroscopy data," in *Proc. 6th IEEE WHISPERS*, Lausanne, Switzerland, Jun. 2014, p. 4.
[33] R. Richter and D. Schläpfer, "Atmospheric/topographic correction for satellite imagery," DLR, Wessling, Germany, Tech. Rep. DLR-IB 565-01, Feb. 2014. [Online]. Available: http://www.rese.ch/pdf/atcor3_manual.pdf
[34] R. Sandau *et al.*, "Design principles of the LH systems ADS40 airborne digital sensor," in *Proc. IAPRS*, 2000, vol. XXXIII, no. Part B1, pp. 258–265.
[35] V. Lund, HySpex—High Resolution, High Speed, Hyperspectral Cameras for Laboratory, Industrial and Airborne Applications, Mar. 2013. [Online]. Available: http://www.hyspex.no/pdfs/HySpex_general.pdf
[36] R. Müller *et al.*, "A program for direct georeferencing of airborne and spaceborne line scanner images," *Int. Archives Photogramm., Remote Sens. Spatial Inf. Sci.*, vol. 34, no. 1, pp. 148–153, 2002.
[37] B. Franch, E. F. Vermote, J. A. Sobrino, and E. Fédèle, "Analysis of directional effects on atmospheric correction," *Remote Sens. Environ.*, vol. 128, pp. 276–288, Jan. 2013.
[38] A. I. Lyapustin *et al.*, "Multi-angle implementation of atmospheric correction for MODIS (MAIAC): 3. Atmospheric correction," *Remote Sens. Environ.*, vol. 127, pp. 385–393, Dec. 2012.

Daniel Schläpfer (M'10) was born in St. Gallen, Switzerland. He received the M.Sc. degree in geography and the Dr.Sc.Nat. and teaching degrees in physics and geography from the University of Zurich, Zurich, Switzerland, in 1994, 1998, and 1999, respectively. He received the Teaching Professor degree from the State of St.Gallen in 2009.

From 1998 to 2008, he was Research Scientist with the Remote Sensing Laboratories, University of Zurich. He is currently with ReSe Applications Schläpfer, Wil, Switzerland. In addition, he holds a physics teaching position with Kantonsschule, Wil. His major fields of research are the geometric preprocessing of airborne scanner data on the basis of the PARGE software, the application of radiative transfer models in imaging spectroscopy, and the advancement of radiometric and atmospheric compensation in the framework of the ATCOR atmospheric correction solution.

Rudolf Richter received the M.Sc. degree in physics from the Technical University of Munich, Munich, Germany, in 1973 and the Dr.Ing. degree in engineering from the Technical University of Dresden, Dresden, Germany, in 1991.

He is currently a Senior Scientist with the Remote Sensing Data Center, German Aerospace Center (DLR), Wessling, Germany, where he is conducting concept development, modeling, and simulation of airborne/spaceborne hyperspectral instruments. It involves advanced techniques and interaction with scientists associated with theory and remote sensing experiments. He developed the ATCOR model, one of the standard codes for atmospheric and topographic correction of multi-/hyperspectral imagery used at universities and research laboratories. His current work focuses on the design of fully automatic processing chains for the evaluation of remotely sensed optical data from the visible to the thermal spectral region.

Tal Feingersh was born in Tel Aviv, Israel. He received the B.A. degree from The Hebrew University of Jerusalem, Jerusalem, Israel, in 1998, the M.Sc. degree from ITC, Enschede, The Netherlands, in 2000, and the Ph.D. degree from Tel Aviv University, Tel Aviv, in 2007.

From 2000 to 2002, he was an Assistant Professor of remote sensing with ITC. From 2008 to 2010, he was with Elbit Systems. He is currently with the MBT Space Division, Israel Aerospace Industries (IAI), Yehud, Israel, where he is concerned with research and development. His research has been concerned with spectral reflectance anisotropy.

Dr. Feingersh is a member of the European Facility for Airborne Research.